Hybrid Energy Storage System With Active Filter Function for Shipboard MVDC System Applications Based on Isolated Modular Multilevel DC/DC Converter

Ran Mo, *Student Member, IEEE*, and Hui Li, *Senior Member, IEEE*

***Abstract*— This paper proposes an isolated modular multilevel dc/dc converter (iM2DC)-based hybrid energy storage system (ESS) for shipboard MVDC grid application. The cell capacitors of the iM2DC are applied to implement the dc active power filter capability, which improves the MVDC bus power quality without auxiliary devices or sacrificing the battery lifetime. In addition, the proposed ESS achieves superior fault response with fault current limiting function, which benefits the fault localization and fast recovery. The operation principle of the proposed system is introduced first and the converter equivalent averaged model is derived. Then the multifunctional control method is presented, including the virtual-impedance-based ripple distribution strategy. Both offline simulation and controller hardware-in-the-loop test results are provided to validate the control strategy as well as the ESS performance.**

***Index Terms*— Active power filter, controller hardware-in-the-loop (CHIL), hybrid energy storage system (ESS); isolated modular multilevel dc/dc converter (iM2DC).**

I. Introduction

MEDIUM-VOLTAGE dc (MVDC) system has gained increasing attention as an alternative to MVAC in shipboard power system (SPS) applications for higher efficiency and flexibility [1], [2]. The navy has already succeeded in fielding ships with a 1 kV MVDC distribution system on board [1]. The energy storage system (ESS) plays an essential role in shipboard MVDC systems to perform as hybrid propulsion energy, provide backup power, buffer large load change, as well as improve power quality in the ship [3]–[5]. The most widely applied nonfuel ESSs in SPS are based on batteries, capacitors, and flywheels [5], which serve at different situations due to their distinct power density and energy density features.

Among the shipboard storage technologies, batteries offer scalable energy storage solutions for high-power and long-term energy demands, as they achieve the highest energy density. Large-scale high power batteries are carried on board to provide alternate propulsion and emergency backup power [6], which are integrated to the shipboard MVDC bus through battery ESS (BESS) converters with specific requirements. These BESS converters have to be designed to operate at both high voltage and high power ratings. Besides, galvanic isolation is recommended for not only safety reasons but also for high voltage conversions [7]. Moreover, due to the lack of mature dc circuit breakers in the MV level, the BESS converter is desired to achieve superior dc fault response, which benefits the MVDC system reliability and resiliency. In addition, considering the high expenses and limited lifetime of today's battery products, multiple services and functions are preferred for BESS from the cost perspective.

High power bidirectional dc/dc converters have been investigated in MV power conversion system applications [8] and can be applied to interface battery storage. Dual-active-bridge (DAB)-type converters are one of the most popular isolated dc/dc converters due to their advantages of galvanic isolation and inherent soft-switching capability [9]. However, the energy contained in the circuit input and output capacitors will result in high short-circuit current under dc line-to-line fault conditions. The converter has to trip to prevent the short circuit from propagating to the other side. Besides, if a single large dc link battery composed of paralleled battery modules is installed, the circulating current existing among battery modules will increase the system loss. Although modular cascaded DAB converter [10]–[12] has been applied to realize the distributed battery module connection, which can suppress the circulating current and achieve higher efficiency, it nevertheless is weak at dc fault response, similar to a single DAB converter. In [13], a modular multilevel DAB-based BESS is proposed with fast fault recovery capability, but it only provides limited functions.

Another potential topology for high power MV BESS application is based on modular multilevel converter (MMC) [14]–[16], while they are mainly focused on the ac grid application. Recently, isolated modular multilevel dc/dc converter (iM2DC) consisting of two MMCs connected through a medium-frequency transformer has been proposed as a dc transformer in HVDC/MVDC grids [17], [18]. Since it follows the similar operation principle of the DAB-type converter, the same issues and limitations will thereby occur

Manuscript received June 22, 2016; revised October 13, 2016 and November 23, 2016; accepted December 5, 2016. Date of publication December 22, 2016; date of current version January 31, 2017. Recommended for publication by Associate Editor Carl N. M. Ho.

The authors are with the Center for Advanced Power Systems, Florida State University, Tallahassee, FL 32310 USA (e-mail: rmo@caps.fsu.edu; hli@caps.fsu.edu).

Color versions of one or more of the figures in this paper are available online at http://ieeexplore.ieee.org.

Digital Object Identifier 10.1109/JESTPE.2016.2642831

when applied in BESS as those of DAB. IM2DC can also be implemented with multilevel modulation [19]–[21]. Although this converter can achieve faster recovery than DAB-type converters [21], it still requires trip actions when fault happens. Furthermore, since all the aforementioned converters lack the instantaneous output current control capability, limited service can be provided, which makes it difficult to maximize the utilization of the batteries.

Meanwhile, since a wide variety of loads including high power propulsion loads and pulsed loads are connected to the MVDC bus through power converters in the shipboard MVDC system, pulsed current and ripple current will be introduced in the MVDC system, which might affect the main rectifier's dynamic behavior or even lead to voltage oscillations on the MVDC bus [22]. One solution to damping these oscillations is installing passive filters, while it is costly and bulky as well as restricted by system configuration [23]. Auxiliary dc active power filters (APFs) [24]–[26] are presented to smooth out MVDC bus voltage ripples and improve overall damping, but the extra device also increases the system cost.

Therefore, the hybrid ESS with dc APF function based on iM2DC is proposed in this paper, which fulfills all the key required characteristics for the MVDC shipboard ESS application. It can achieve both fault current limiting and fault ride through functions with its dc current direct control capability, so it is possible to maintain operation during fault to provide fault localization and fast recovery. Besides, via virtual impedance method, the proposed topology employs the converter cell capacitors rather than batteries to provide ripple energy to achieve APF function, which allows ESS to improve MVDC system power quality without consuming battery lifetime or extra circuits. In addition, since the medium frequency transformer operation frequency is as high as the converter switching frequency, the whole system power density can be improved.

This paper is organized as follows. Section II describes the proposed iM2DC-based ESS topology and derives its equivalent model. The operation principle of the hybrid ESS is also explained. Section III introduces its control strategy aiming at multifunctions, including the implementation of injecting ripples from capacitor storage rather than batteries. Then in Section IV, both offline simulation and controller hardware-in-the-loop (CHIL) test are conducted to verify the capability of proposed technology and Section V summarizes the main conclusions.

II. Proposed iM2DC-Based ESS System

A. System Topology and Operation Principle

Fig. 1 presents the proposed iM2DC-based ESS system topology integrated to the MVDC bus, which consists of one single-phase MMC in the high voltage side (HVS) and one single-phase cascaded converter in the low voltage side (LVS). Full bridge cells are employed on both the sides, where distributed battery storage units and capacitors are installed at the dc link of each cell in the LVS and HVS, respectively. HVS and LVS are connected through a medium frequency ac transformer to satisfy the galvanic isolation requirement.

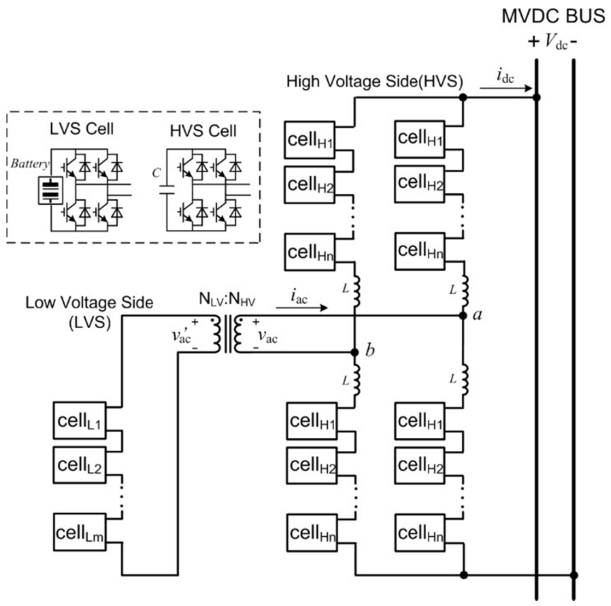

Fig. 1. Proposed iM2DC-based ESS topology.

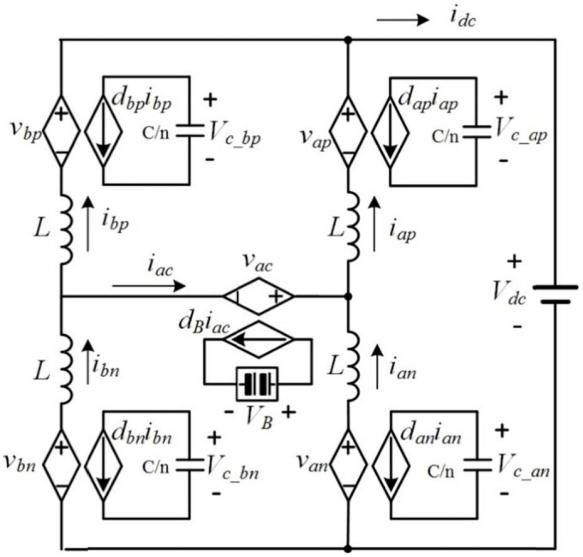

Fig. 2. Averaged model of proposed iM2DC.

The high transformer operation frequency which equals the switching frequency leads to reduced passive elements size as well.

Phase shift sinusoidal pulsewidth modulation method is applied to produce quasi-sinusoidal waveforms at the transformer side of the iM2DC. Since the ESS converter is controlled as a current source from the MVDC side, it allows multiple functions compared to other high power isolated dc/dc converter such as DAB-type converters. Therefore, it is possible to implement the APF function by injecting the compensated ripple power to smooth the MVDC bus current. In addition, the converter current remains controllable during fault, which protects the ESS from destructive overcurrent without tripping.

Fig. 2 illustrates the averaged model of proposed iM2DC referred to the HVS considering ideal transformer's

characteristics. For the HVS, the n cells at the positive and negative arms are combined and modeled as voltage sources v_{xp} and v_{xn} separately ($x = a, b$). L denotes the arm inductor; V_{c_xp} and V_{c_xn} denote the total equivalent capacitor voltage in the positive and negative arm; and v_{ac} and i_{ac} represent the ac side voltage and current, respectively. There is also circulating current flowing in HVS if unbalanced condition occurs. In the following analysis, only balanced condition is considered. The LVS modeling is similar to HVS and V_B is the total equivalent battery voltage referring to HVS.

If considering the dc and ac source separately, the converter state equation can be derived as

$$\begin{cases} V_{dc} = -L\dfrac{d\sum_{x=a,b}(i_{xp}+i_{xn})}{2dt} \\ \qquad\quad + \dfrac{1}{2}\sum_{x=a,b}(v_{xp}+v_{xn}) \\ v_{ac} = L\dfrac{d(i_{ap}-i_{bp}-i_{an}+i_{bn})}{2dt} \\ \qquad\quad + \dfrac{1}{2}(v_{bp}-v_{ap}+v_{an}-v_{bn}) \\ \dfrac{C}{n}\dfrac{v_{c\_xp}}{dt} = -d_{xp}\cdot i_{xp}, \quad \dfrac{C}{n}\dfrac{dv_{c\_xn}}{dt} = -d_{xn}\cdot i_{xn} \end{cases} \tag{1}$$

where d_{xp} and d_{xn} denote the duty ratios of the positive and negative arms in phase leg x. From (1) we can see that the arm voltage contains both the dc and ac components. Then the duty ratio in each arm can be written as

$$d_{ap} = d_{bn} = d_{dc} - d_{ac}, d_{an} = d_{bp} = d_{dc} + d_{ac}. \tag{2}$$

The arm current can be obtained from dc current i_{dc} and ac current i_{ac} if balanced as

$$i_{ap} = i_{bn} = \frac{1}{2}i_{dc} + \frac{1}{2}i_{ac}, i_{an} = i_{bp} = \frac{1}{2}i_{dc} - \frac{1}{2}i_{ac}. \tag{3}$$

Substituting (2) and (3) into (1) and reorganizing the results yield

$$\begin{cases} V_{dc} = -L\dfrac{di_{dc}}{dt} + d_{dc}\cdot v_\Sigma + d_{ac}\cdot v_\Delta \\ v_{ac} = L\dfrac{di_{ac}}{dt} + d_{ac}\cdot v_\Sigma + d_{dc}\cdot v_\Delta \\ \dfrac{C}{n}\dfrac{dv_\Sigma}{dt} = -d_{dc}\cdot i_{dc} + d_{ac}\cdot i_{ac} \\ \dfrac{C}{n}\dfrac{dv_\Delta}{dt} = -d_{ac}\cdot i_{dc} + d_{dc}\cdot i_{ac} \end{cases} \tag{4}$$

where v_Σ and v_Δ are the sum and the difference of equivalent capacitor voltages in the positive and negative arms, respectively. Accordingly, the equivalent averaged model of the proposed iM2DC converter can be developed as in (4) and demonstrated in Fig. 3. The HVS model includes one dc current loop controlling power exchange with MVDC bus, one ac current loop transferring power between HVS and LVS, one-phase capacitor dynamic model describing the HVS capacitor power, and one fundamental ripple model related to the fundamental ripple effects. The LVS model controls the battery energy at LVS.

B. Hybrid ESS Configuration

The cell capacitors at HVS can act as energy storage components as capacitor voltages are allowed to vary within a large range, therefore the iM2DC can be controlled as a hybrid energy storage converter, which is another advantage of the proposed system. The hybrid ESS structure is demonstrated in Fig. 4 based on the derived system equivalent averaged model. It shows that the energy exchanged between batteries and the MVDC system will flow through HVS capacitors. As a hybrid ESS converter with direct current control capability, the iM2DC can control the charging and discharging current distribution between LVS batteries and HVS cell capacitors, which makes it possible to utilize the more suitable energy storage element according to the system demands.

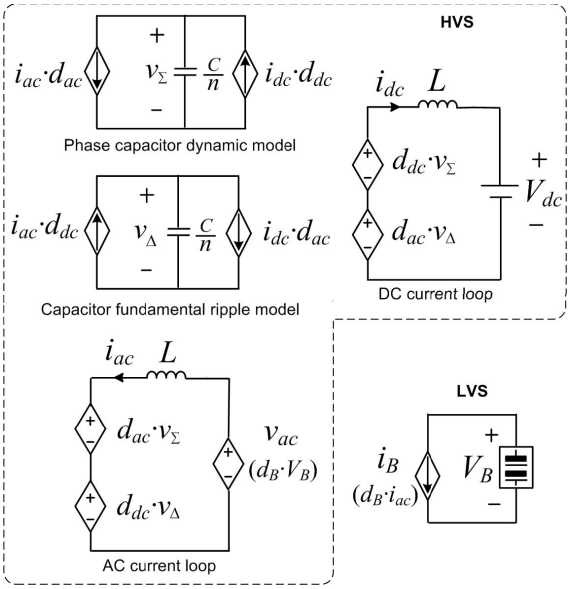

Fig. 3. Equivalent averaged model of the proposed iM2DC.

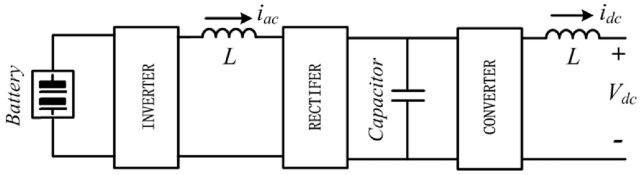

Fig. 4. Equivalent structure of proposed hybrid ESS.

The battery manufacturer recommends the ripple current to be limited to the 20 h discharge rate (C/20) [27] since the temperature rises and expected lifetime decays with the increasing of ripple current [27], [28]. For example, in the valve regulated lead acid battery, three times of the rating ripple current will lead to almost 1 °F heating and battery lifetime reduction by approximately 3% [27]. Normally the batteries will not be used for APF applications since the introduced battery current ripple will likely exceed the recommended ripple current range. In addition, using batteries for APF will cost extra columns especially when no energy is demanded by the SPS energy management system (EMS). The used coulomb will be reflected in the battery changed state-of-health [29], and will further aggravate battery aging. However, with the proposed hybrid ESS, capacitors can be employed instead of batteries to provide the ripple energy for the APF function.

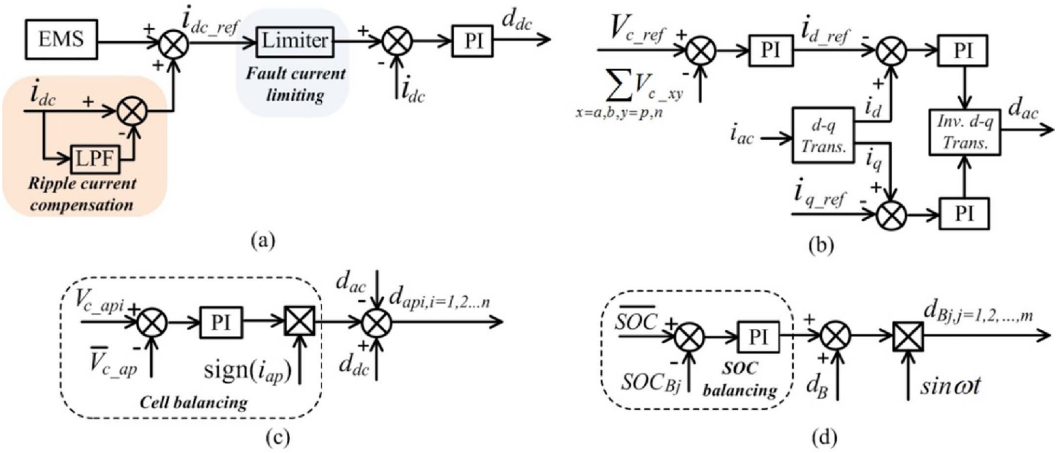

Fig. 5. Proposed ESS control diagram. (a) HVS dc current control. (b) HVS ac current control. (c) HVS cell duty ratio generation. (d) LVS cell duty ratio generation.

In this case, the battery ripple current will be significantly decreased and no extra columns will be wasted during APF, hence, the battery lifetime can be extended. Furthermore, due to the capacitor's smaller output impedance than that of the battery, the system efficiency can be improved as well by distributing the ripple current to capacitors. Thus, the MVDC bus power quality will be improved without sacrificing the battery lifetime or auxiliary devices.

III. Multifunctional Control Strategy

A. Proposed Control Method

The whole control strategy is divided into HVS and LVS control. The HVS aims at multiobjectives of superior fault performance and APF by regulating the converter current; the LVS provides transformer side sinusoidal voltage. Moreover, the derived converter equivalent averaged model reveals that the dc current and ac current of HVS can be controlled individually.

The proposed iM2DC-based ESS control method diagram is depicted in Fig. 5. At the HVS stage, the dc current is controlled to transfer energy between the batteries and grid with the command from EMS as shown in Fig. 5(a). The commanded value is compensated with the whole dc current ripple extracted from the measured MVDC current by setting the low-pass filter cutoff frequency to 1 Hz. Then the ripple compensated command will be sent to the dc current controller as the reference. Consequently, the converter will not only charge and discharge the batteries as the SPS request, but also accomplish APF function by injecting the bus ripple current. Another task of the HVS control is to maintain operation during fault for the purpose of fault localization and fast recovery, so a fault current limiter is installed to protect the equipment from overcurrent during fault, and the fault current will be limited to any level even zero as system required. On the other hand, ac current is used to stabilize the total capacitor voltage with traditional single-phase dual-loop *d-q* vector control as shown in Fig. 5(b), where V_{c_ref} denotes the total HVS capacitor voltage reference and ΣV_{c_xy} $(x = a, b; y = p, n)$ is the sum of HVS measured capacitor voltages.

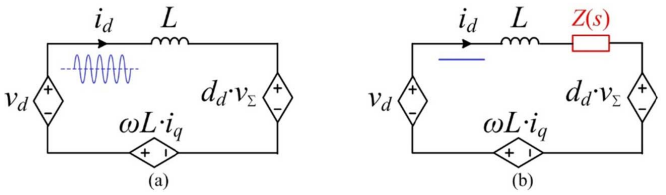

Fig. 6. IM2DC d vector model of ac current. (a) Original model. (b) With extra impedance $Z(s)$.

With dc and ac duty ratios generated from the PI controllers, the arm duty ratio is obtained according to (2). The individual cell duty ratio of each arm $d_{xyi}(i = 1, 2, \ldots, n)$ is composed of the arm duty ratio and cell balancing compensation, which is illustrated in Fig. 5(c) taking the positive arm at phase leg a as an example. The ith cell capacitor voltage V_{c_api} is adjusted to follow the averaged cell capacitor voltage $\bar{V}_{c\_ap}$. It is noted that the cell balancing control is based on the arm current, so the polarity of the arm current has to be included. At the LVS stage shown in Fig. 5(d) where ω is the transformer current angular frequency, open loop control is adopted to give the jth $(j = 1, 2, \ldots, m)$ cell duty ratio, the SOC balancing is realized as well by controlling the battery module SOC of each cell to track the averaged SOC.

B. APF With Extended Battery Lifetime

During APF, the ripple may propagate to LVS batteries if no specific actions are taken. In order to avoid the adverse impacts of low frequency ripple component on battery lifetime, the hybrid ESS has to distribute ripple energy to the HVS capacitors. Although the battery current may contain low frequency ripple components, there will be no ripple component existing in ac current but an ac current magnitude variation. Nevertheless, the ripple component will exist in the d vector component of ac current, which makes *d-q* vector control very suitable for the hybrid ESS ac loop control.

Virtual-impedance-based strategy is performed for the ripple distribution. Fig. 6(a) presents the iM2DC converter d vector model of ac current loop in *d-q* frame from the derived

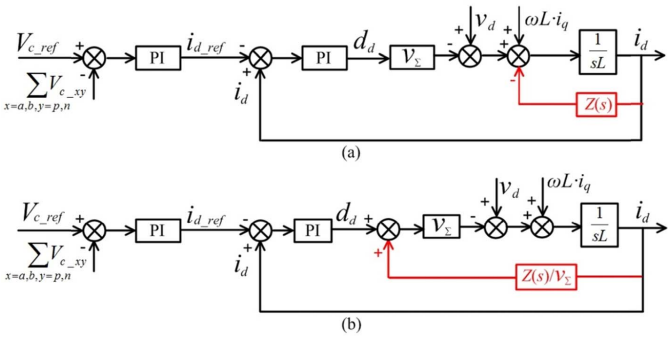

Fig. 7. Control diagram of ac current in d vector. (a) With extra impedance $Z(s)$. (b) Equivalent diagram.

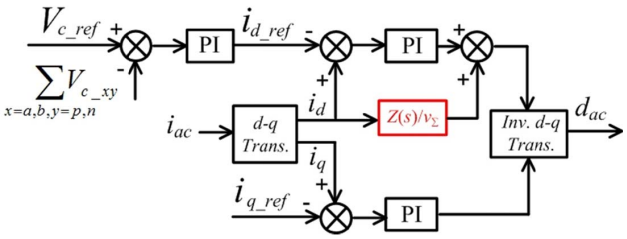

Fig. 8. Improved HVS ac current control with the virtual impedance.

equivalent averaged model regardless of the capacitor voltage difference v_Δ. v_d, i_d and d_d represent the d vector of transformer voltage, current, and ac duty ratio, respectively. To prevent ripple components occurring in i_d and further flowing into the batteries side, the impedance of d vector current path at the ripple frequency should be high enough compared to the dc current path. However, the arm inductor L is designed at the transformer frequency, which equals the cell switching frequency, so its impedance at low ripple frequency is relatively small. Therefore, extra impedance $Z(s)$ needs to be added in series with L as shown in Fig. 6(b), to increase the d vector loop impedance.

Based on the HVS ac current control in Fig. 5(b) and the d vector plant model with $Z(s)$ in Fig. 6(b), the control block diagram of the ac current in d vector is provided in Fig. 7(a). By moving one of the feedback nodes of i_d forward to the output of inner loop PI controller and refine the corresponding feedback gain, the equivalent control diagram can be as given in Fig. 7(b).

Accordingly, the HVS ac current control can be modified as shown in Fig. 8, where feeding i_d back with the gain Z(s)/V_Σ is equivalent to adding a virtual impedance Z(s) in series with the ac inductor. There is no modification in the q vector of ac current control since there is no ripple component in the q vector model. The Z(s) has to perform high impedance at ripple frequency and low impedance at dc, so a first-order high pass filter is selected to act as the virtual impedance Z(s). The cutoff frequency is set to be 10 Hz. In the shipboard MVDC system, most of the ripples are produced by the nonlinear load, pulse rectifier, and the interactions among converters, which are usually higher than 10 Hz. Therefore, this design should be applicable under most working conditions.

TABLE I
PSIM SIMULATION PARAMETERS

Parameters	Specifications
MVDC bus voltage V_{dc}	6000V
HVS cell number n	6
LVS cell number m	6
Cell capacitor voltage in HVS	1000V
Cell capacitor C	200μF
Arm inductor L	50μH
Transformer turns ration N_{LV}:N_{HV}	1:4
Transformer peak voltage on HVS	6000V
Rated battery module voltage	320V
Nominal battery-unit capacity	300Ah
Transformer frequency	10kHz
Cell switching frequency	10kHz
HVS switching device	FF150R12RT4
LVS switching device	FF600R06ME3

IV. SIMULATION AND CHIL VERIFICATION

A. Offline Simulation Verification

Offline simulation was conducted first to validate the functionality of proposed hybrid ESS. A 500 kW iM2DC-based ESS model connected to a 6 kV shipboard MVDC bus was built in PSIM with the main parameters listed in Table I.

Fig. 9(a) gives the key waveforms during steady-state operation when the batteries are discharged to provide energy to the MVDC grid. Fig. 9(b) describes the system performance when the line-to-line fault happens at the MVDC side and the bus voltage drops to zero, the simulation results show that the converter fault current can be limited at 200 A and the converter will retain operation instead of tripping. Moreover, the energy stored in both batteries and HVS capacitors can be released to serve as short-time uninterruptible power supply if necessary.

The proposed hybrid ESS-based APF function was validated via offline simulation as well. In the simulation, one 100 Hz pulsed load and one load containing 180 Hz harmonics were connected to the MVDC, then the MVDC bus exhibited low frequency ripple current. Fig. 10 provides the MVDC bus current, load current, and the BESS converter compensation current waveforms. The results show that after the APF function is enabled, the converter current flowing into MVDC bus provides the needed ripple component no matter whether there is power exchange between batteries and MVDC system or not. As a result, the MVDC bus current will be smoothed. However, APF leads to extra battery consumptions even without power demand from EMS as shown in Fig. 10(a) and corresponding ripples on batteries during discharging as shown in Fig. 10(b), which compromises the battery lifetime under either scenario.

Fig. 11 verifies the effectiveness of proposed virtual-impedance-based method in the hybrid ESS. In this iM2DC-

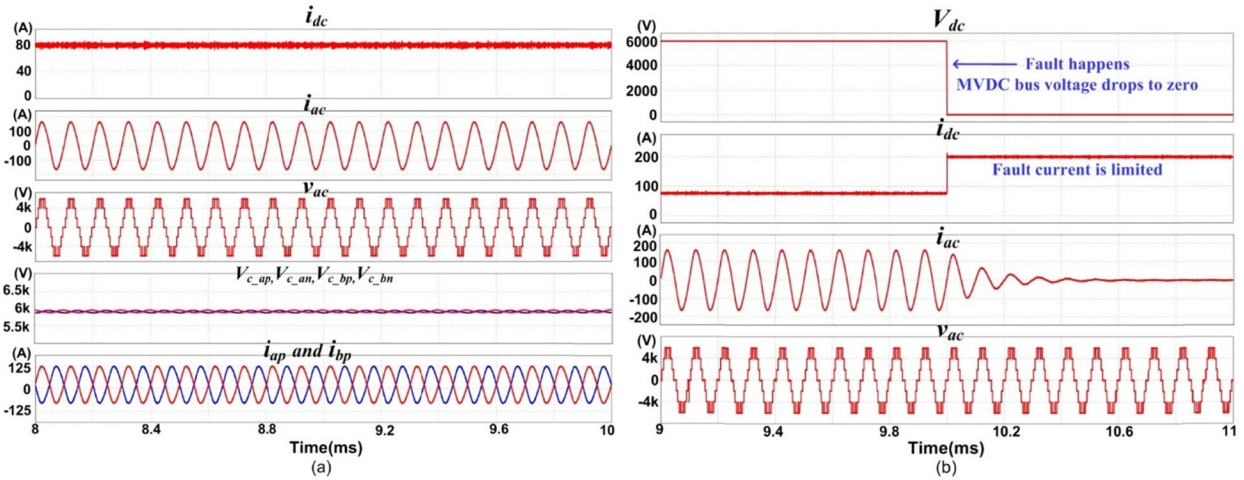

Fig. 9. PSIM simulation results. (a) Steady-state operation. (b) Fault current limiting.

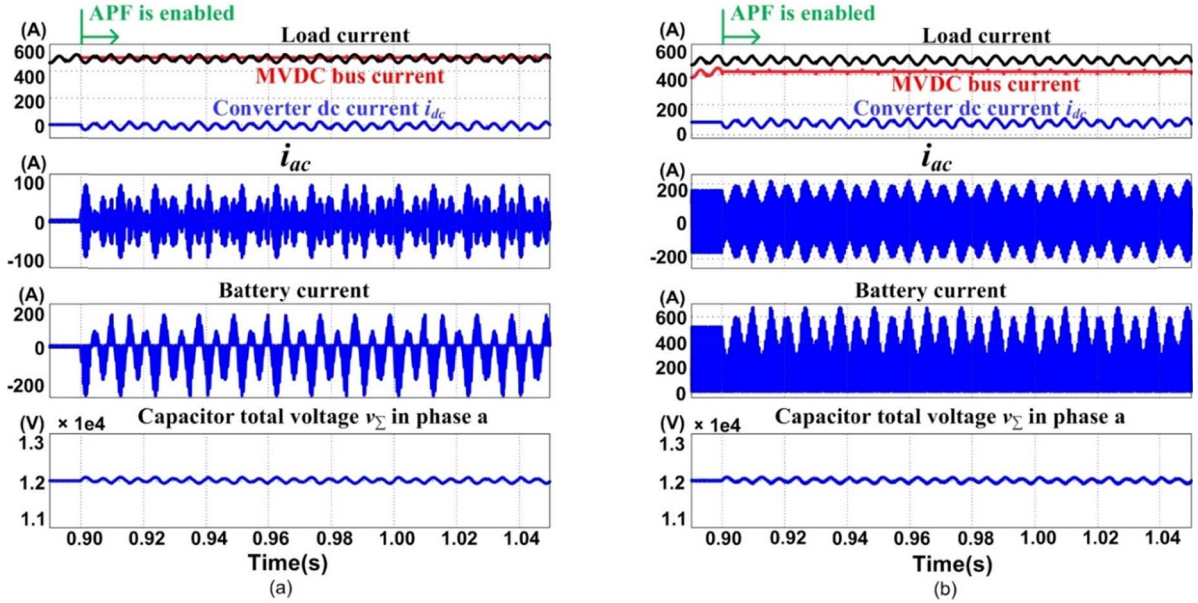

Fig. 10. Offline simulation results of APF function without virtual impedance. (a) No power exchange. (b) Batteries are discharging.

based ESS, the recommended ripple current C/20 is around 15 A. Higher ripple will generate heat and negative effects on battery lifetime as discussed in Section II. In practice, the battery modules are usually connected in parallel with a small capacitor to filter out the high frequency ripple, including the double fundamental frequency and switching frequency ripples at the battery side of the iM2DC-based ESS. However, the low frequency ripple introduced by APF function will still remain and sacrifice the battery lifetime. Therefore, only 100 and 180 Hz components are considered from the simulation results to evaluate the adverse impact of ripples on the battery lifetime. The simulation results from Fig. 10 show that the RMS value of low frequency battery ripple current is around 72A for both (a) and (b), which is almost five times of rating. With the proposed virtual-impedance shown in Fig. 11, the low frequency battery ripple current RMS reduces to 11A, which is within the recommended ripple current range. Moreover, Fig. 12 provides the FFT analysis results of battery current in Figs. 10(b) and11(b). With the proposed virtual-impedance-based method, the corresponding 100 and 180 Hz ripple component percentages are reduced from 10% and 32.7% in Fig. 12(a) to 2.3% and 4.3% in Fig. 12(b), respectively. The case under no power exchange reveals similar results, wherein the battery ripple components in Fig. 11(a) reduced by 77% at 100 Hz and 86.9% at 180 Hz from those in Fig. 10(a). The reduction of the battery ripple current RMS in both the scenarios indicates that the proposed virtual-impedance strategy will inhibit temperature rise and benefit the extending of battery lifetime.

B. CHIL Verification

In order to investigate the feasibility of the proposed technology, the pure offline simulation might not reveal all the salient characteristics sufficiently, while the system prototyping and hardware experiment may be rather costly and time-consuming because of its high power and high voltage ratings. Thus, the CHIL methodology offers an efficient and

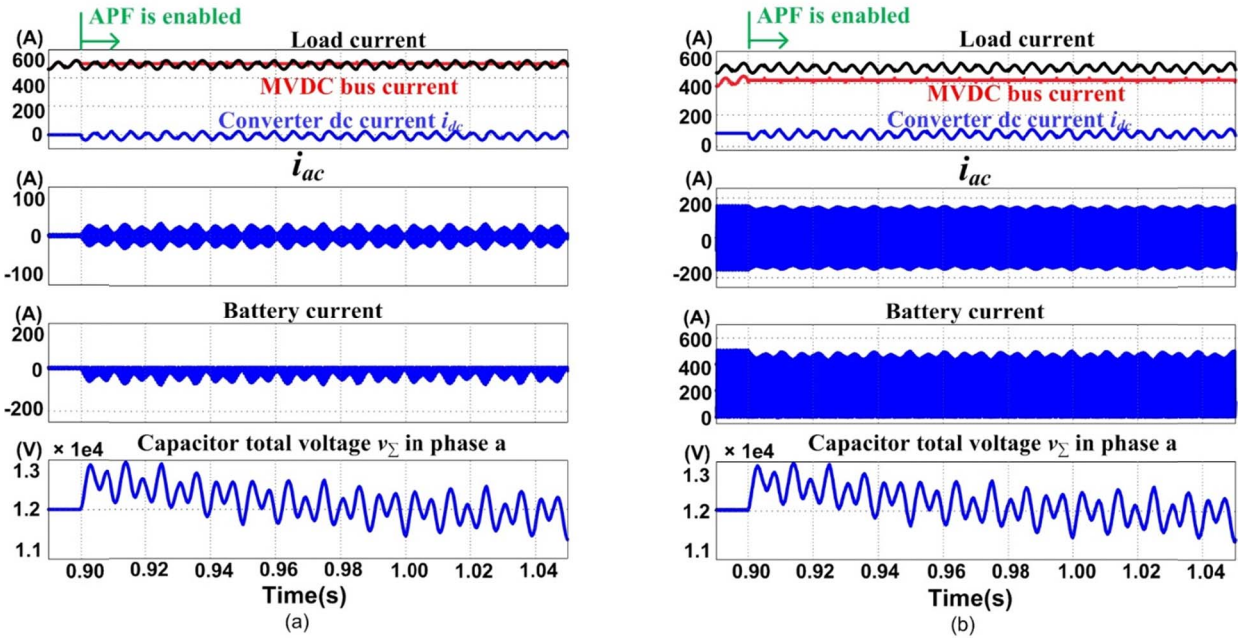

Fig. 11. Offline simulation results of APF function with virtual impedance. (a) No power exchange. (b) Batteries are discharging.

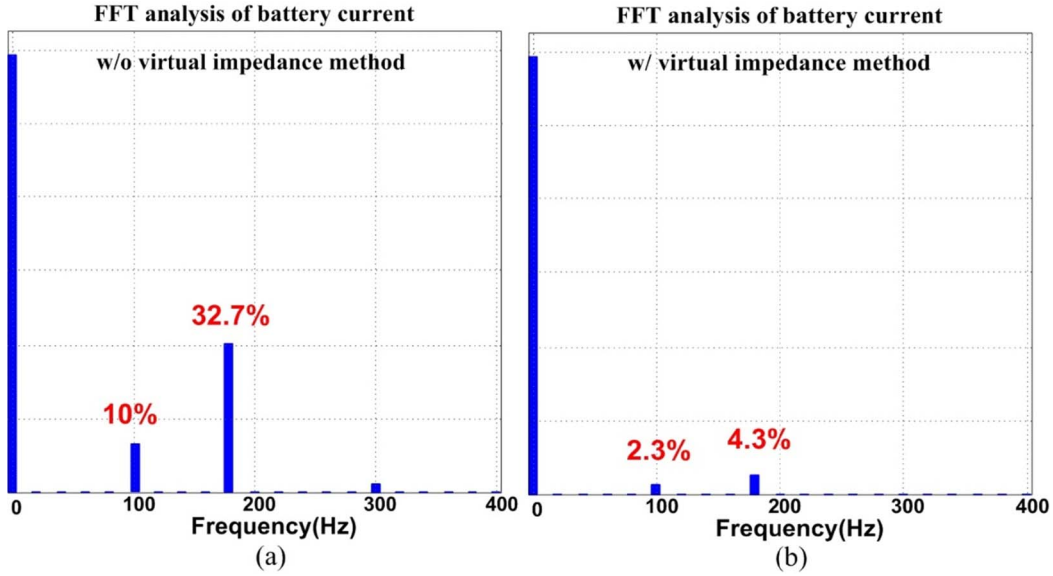

Fig. 12. FFT analysis results of battery current during APF when discharging. (a) Without proposed virtual-impedance method. (b) With proposed virtual-impedance method.

practical approach to verify the control strategy as well as the converter performance due to its low cost, low risk, high flexibility, and rapid realization [30]. A CHIL testbed available in the authors' lab, which has been proven to be consistent with the pure hardware results [31], was used to verify the proposed ESS operation and APF function.

Fig. 13 presents the CHIL testbed configuration, including the controller hardware executing the control strategies and real-time simulation platform simulating MVDC grid with iM2DC-based ESS model. The controller hardware comprises of several components interconnected via fiber optics as explained in Fig. 13(a). The system is based on the ABB AC800PEC product line and has been described in [31]. One master controller receives the external converter reference from the real-time simulator through the Combi I/O device and sends the reference information to the slave level. Another AC800PEC product is employed as slave controller, which implements the control strategies with the converter measured values from PEC measuring interface (PECMI) as feedback. The generated converter modulation waveforms are broadcast to the individual DSP-based cell controllers by the control HUB. Then the PWM signals are produced in the cell controllers. These PWM pulses are received by the converter model simulated in the Real Time Digital Simulator (RTDS) via the digital input (Giga-Transceiver Digital Input) interface card as demonstrated in Fig. 13(b). With the ESS model running in RTDS at a time step of 3μs, the system voltage and current as well as the reference from EMS is measured

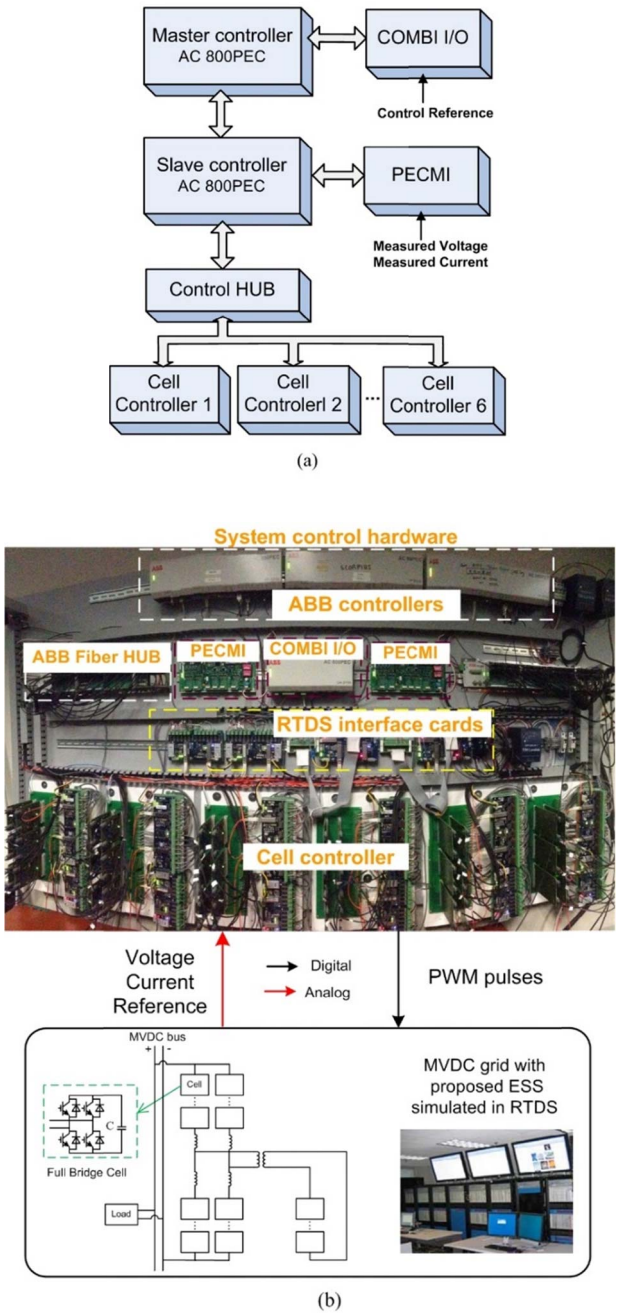

Fig. 13. CHIL testbed. (a) Controller hardware structure. (b) CHIL configuration.

and output through the D/A conversion (Giga-Transceiver Analog Output) interface card to the PECMI and COMBI I/O, respectively.

Most of the CHIL simulation specifications are similar to those of the offline simulation. However, since the sampling frequency of the applied controller hardware is limited, the highest transformer frequency achievable with sinusoidal waveforms is around 400 Hz. In the CHIL simulation results below, the transformer frequency was further reduced to 200 Hz. Thus, the arm inductor and cell capacitors also had to be increased. Table II provides the key parameters of CHIL system, which differ from those of the offline simulation. Even with such a compromise, the main functionality and

TABLE II
CHIL SIMULATION KEY PARAMETERS

Parameters	Specifications
Transformer frequency	200Hz
Cell switching frequency	2kHz
Cell capacitor C	2mF
Arm inductor L	2.5mH

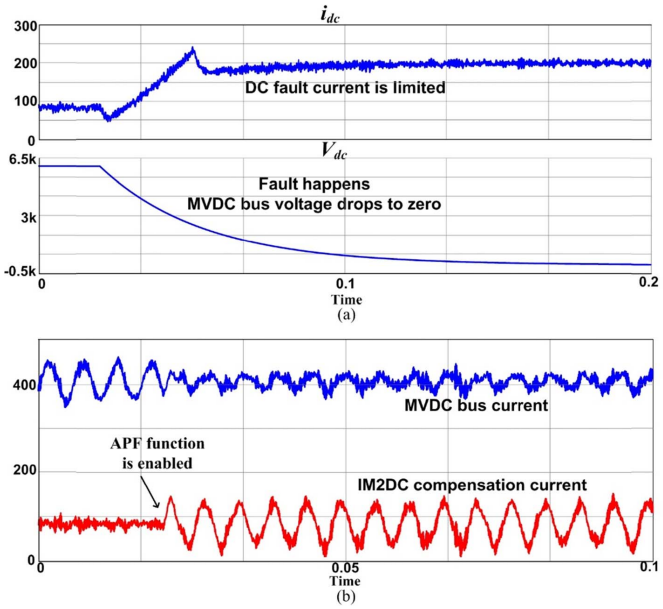

Fig. 14. CHIL simulation results. (a) Fault current limiting. (b) APF.

operation of the proposed ESS technology could be verified. The proposed control strategy is modified from the embedded basic converter control in the commercial control hardware, which can be found in [31].

Fig. 14(a) verifies the fault current limiting capability of the proposed ESS. It shows that when the bus voltage drops to zero under fault condition, the converter can maintain operation and provide stable dc current limited at any desired level rather than tripping. Fig. 14(b) demonstrates the CHIL results of the MVDC bus current and the iM2DC dc current. A load containing 180 Hz ripple is connected to the grid. Similar to the offline simulation results, after the APF function is enabled, the iM2DC generates corresponding ripple current to compensate the bus current ripple. Consequently, the MVDC bus current ripple becomes less severe.

V. CONCLUSION

A hybrid ESS based on iM2DC is proposed for the shipboard MVDC application in this paper. A multifunctional control algorithm is developed to achieve energy supplement, APF, and fault current limiting. With the proposed virtual-impedance-based strategy, the converter cell capacitors are utilized to realize APF without compromising the battery

lifetime. The simulation results indicate that the proposed ESS technology is capable of improving the power quality and fault protection for shipboard MVDC applications with higher power density and reduced control complexity. The CHIL test results further validate the ESS control design for both steady state and dynamic changes. With the proposed technology, the steady-state power quality of the shipboard MVDC system can be improved more efficiently without bulky filter banks or auxiliary devices.

REFERENCES

[1] T. Ericsen, "The ship power electronic revolution: Issues and answers," in *Proc. 55th Annu. IEEE Petroleum Chem. Ind. Committee Tech. Conf.*, Cincinnati, OH, USA, Sep. 2008, pp. 1–11.

[2] T. Ericsen, "Engineering 'total electric ship,"' in *Proc. 54th Annu. IEEE Petroleum Chem. Ind. Committee Tech. Conf.*, Sep. 2007, pp. 1–6.

[3] A. T. Elsayed and O. A. Mohammed, "A comparative study on the optimal combination of hybrid energy storage system for ship power systems," in *Proc. IEEE Electr. Ship Technol. Symp.*, Jun. 2015, pp. 140–144.

[4] J. Hou, J. Sun, and H. Hofmann, "Interaction analysis and integrated control of hybrid energy storage and generator control system for electric ship propulsion," in *Proc. Amer. Control Conf.*, Chicago, IL, USA, 2015, pp. 4988–4993.

[5] Y. Tang and A. Khaligh, "Bidirectional hybrid battery/ultracapacitor energy storage systems for next generation MVDC shipboard power systems," in *Proc. IEEE Vehicle Power Propuls. Conf.*, Chicago, IL, USA, Sep. 2011, pp. 1–6.

[6] R. Hebner. (Apr. 2014). Energy storage on future electric ships. The Office of Naval Research. [Online]. Available: https://www.utexas.edu/research/cem/Energy_storage_photos/Energy%20Storage%20on%20Future%20Electric%20Ships.pdf

[7] *IEEE Recommended Practice for 1 kV to 35 kV Medium-Voltage DC Power Systems on Ships*, IEEE Standard 1709-2010, Nov. 2010.

[8] S. Inoue and H. Akagi, "A bidirectional isolated DC–DC converter as a core circuit of the next-generation medium-voltage power conversion system," *IEEE Trans. Power Electron.*, vol. 22, no. 2, pp. 535–542, Mar. 2007.

[9] N. Soltau, R. U. Lenke, and R. W. De Doncker, *High-Power DC-DC Converter* (E.ON Energy Research Center Series), vol. 5, no. 5. Aachen, Germany: RWTH Aachen Univ., Sep. 2013.

[10] G. Ortiz, J. Biela, D. Bortis, and J. W. Kolar, "1 megawatt, 20 kHz, isolated, bidirectional 12kV to 1.2kV DC-DC converter for renewable energy applications," in *Proc. Int. Power Electron. Conf.*, 2010, pp. 3212–3219.

[11] M. Bragard, N. Soltau, S. Thomas, and R. W. De Doncker, "The balance of renewable sources and user demands in grids: Power electronics for modular battery energy storage systems," *IEEE Trans. Power Electron.*, vol. 25, no. 12, pp. 3049–3056, Dec. 2010.

[12] S. Thomas, M. Stieneker, and R. W. De Doncker, "Development of a modular high-power converter system for battery energy storage systems," in *Proc. Eur. Conf. Power Electron. Appl.*, 2011, pp. 1–10.

[13] Y. Shi, R. Li, and H. Li, "Modular multilevel dual active bridge DC-DC converter with ZVS and fast DC fault recovery for battery energy storage systems," in *Proc. IEEE Appl. Power Electron. Conf. Expo.*, Mar. 2016, pp. 1675–1681.

[14] L. Zhang, F. Gao, N. Li, Q. Zhang, and C. Wang, "Interlinking modular multilevel converter of hybrid AC-DC distribution system with integrated battery energy storage," in *Proc. IEEE Energy Convers. Congr. Expo.*, Montreal, QC, Canada, Sep. 2015, pp. 70–77.

[15] F. Guo and R. Sharma, "A modular multilevel converter with half-bridge submodules for hybrid energy storage systems integrating battery and ultracapacitor," in *Proc. IEEE Appl. Power Electron. Conf. Expo.*, Charlotte, NC, USA, Mar. 2015, pp. 3025–3030.

[16] A. Hillers and J. Biela, "Optimal design of the modular multilevel converter for an energy storage system based on split batteries," in *Proc. 15th Eur. Conf. Power Electron. Appl.*, Sep. 2013, pp. 1–11.

[17] I. A. Gowaid, G. P. Adam, A. M. Massoud, S. Ahmed, D. Holliday, and B. W. Williams, "Quasi two-level operation of modular multilevel converter for use in a high-power DC transformer with DC fault isolation capability," *IEEE Trans. Power Electron.*, vol. 30, no. 1, pp. 108–123, Jan. 2015.

[18] I. A. Gowaid, G. P. Adam, S. Ahmed, D. Holliday, and B. W. Williams, "Analysis and design of a modular multilevel converter with trapezoidal modulation for medium and high voltage DC-DC transformers," *IEEE Trans. Power Electron.*, vol. 30, no. 10, pp. 5439–5457, Oct. 2015.

[19] S. Kenzelmann, A. Rufer, D. Dujic, F. Canales, and Y. R. De Novaes, "Isolated DC/DC structure based on modular multilevel converter," *IEEE Trans. Power Electron.*, vol. 30, no. 1, pp. 89–98, Jan. 2015.

[20] S. Kenzelmann, A. Rufer, D. Dujic, F. Canales, and Y. R. de Novaes, "A versatile DC/DC converter based on modular multilevel converter for energy collection and distribution," in *Proc. IET Conf. Renew. Power Generat.*, 2011, pp. 1–6.

[21] S. Kenzelmann, "Modular DC/DC converter for DC distribution and collection networks," Ph.D. dissertation, Ind. Electron. Lab., Swiss Federal Inst. Technol., Lausanne, Lausanne, Switzerland, 2012.

[22] T. Ericsen, N. Hingorani, and Y. Khersonsky, "Power electronics and future marine electrical systems," *IEEE Trans. Ind. Appl.*, vol. 42, no. 1, pp. 155–163, Jan./Feb. 2006.

[23] S. D. Sudhoff, K. A. Corzine, S. F. Glover, H. J. Hegner, and H. N. Robey, Jr., "DC link stabilized field oriented control of electric propulsion systems," *IEEE Trans. Energy Convers.*, vol. 13, no. 1, pp. 27–33, Mar. 1998.

[24] H. Mirzaee, S. Dutta, and S. Bhattacharya, "A medium-voltage DC (MVDC) with series active injection for shipboard power system applications," in *Proc. IEEE Energy Convers. Congr. Expo.*, Sep. 2010, pp. 2865–2870.

[25] H. Mirzaee, B. Parkhideh, and S. Bhattacharya, "Design and control of series DC active filter (SDAF) for Shipboard medium-voltage DC power system," in *Proc. IEEE Electr. Ship Technol. Symp.*, Apr. 2011, pp. 452–458.

[26] H. Mirzaee, S. Bhattacharya, and S. Bala, "A multi-loop control system for series DC active filter in a medium-voltage DC amplifier," in *Proc. IEEE Energy Convers. Congr. Expo.*, Sep. 2013, pp. 15–19.

[27] Emerson Network Power. (2015). *Effects of AC Ripple Current on VRLA Battery Life From Emerson Network Power*, accessed on 2015. [Online]. Available: http://bit.ly/sq0xnG

[28] A. J. Ruddell *et al.*, "Analysis of battery current microcycles in autonomous renewable energy systems," *J. Power Sour.*, vol. 112, pp. 531–546, Nov. 2002.

[29] Y. Yang, H. Li, A. Aichhorn, J. Zheng, and M. Greenleaf, "Sizing strategy of distributed battery storage system with high penetration of photovoltaic for voltage regulation and peak load shaving," *IEEE Trans. Smart Grid*, vol. 5, no. 2, pp. 982–991, Mar. 2014.

[30] J. L. Burbank, W. Kasch, and J. Ward, "Hardware-in-the-loop simulations," in *An Introduction to Network Modeling and Simulation for the Practicing Engineer*, 1st ed. Hoboken, NJ, USA: Wiley, 2011, pp. 114–142.

[31] M. M. Steurer *et al.*, "Multifunctional megawatt-scale medium voltage DC test bed based on modular multilevel converter technology," *IEEE Trans. Transport. Electrific.*, vol. 2, no. 4, pp. 597–606, Dec. 2016.

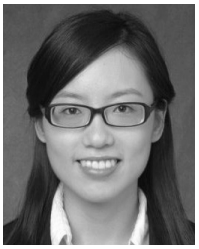

Ran Mo (S'14) received the B.S. degree in electrical engineering from Southeast University, Nanjing, China, in 2010, and the M.S. degree in electrical engineering from the Huazhong University of Science and Technology, Wuhan, China, in 2013. She is currently pursuing the Ph.D. degree with the Department of Electrical and Computer Engineering, Florida State University, Tallahassee, FL, USA.

Her current research interests include modular multilevel converters and hardware-in-the-loop simulation.

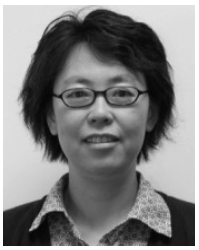

Hui Li (S'97–IM'00–SM'01) received the B.S. and M.S. degrees in electrical engineering from the Huazhong University of Science and Technology, Wuhan, China, in 1992 and 1995, respectively, and the Ph.D. degree in electrical engineering from the University of Tennessee, Knoxville, TN, USA, in 2000.

She is currently a Professor with the Department of Electrical and Computer Engineering, College of Engineering, Florida State University, Tallahassee, FL, USA. Her current research interests include bidirectional dc-dc converters, modular multilevel converters, and photovoltaic converters applying widebandgap device.